DIFFRACTION CONTRAST FROM DISSOCIATED FRANK DISLOCATIONS

I. COMPUTED ELECTRON MICROGRAPHS

By L. M. Clarebrough* and A. J. Morton*

[*Manuscript received December* 19, 1968]

Summary

The influence of degree of dissociation on the diffraction contrast from a Frank dislocation for 111, 220, and 020 reflections has been investigated using the technique devised by Head and Humble for computing electron microscope images.

The diffraction contrast from a dissociated Frank dislocation differs in several ways from that of an undissociated dislocation. For 111 reflections, strong contrast occurs when $\boldsymbol{g}.\boldsymbol{u} \neq 0$. For 220 reflections, images are single and continuous with strong contrast on one side only. The strong contrast does not invert from side to side for $+\boldsymbol{g}$ and $-\boldsymbol{g}$. For 020 reflections the extent to which reversal of contrast occurs in $\pm\boldsymbol{g}$ is a function of $\boldsymbol{g}$, the beam direction, and the separation of the Shockley and stair-rod dislocations.

The computations for an undissociated Frank dislocation are in general agreement with previous computations, but indicate that a Frank dislocation may show strong contrast for certain beam directions when $\boldsymbol{g}.\boldsymbol{b} = \pm\frac{1}{3}$.

I. Introduction

The diffraction contrast from undissociated Frank dislocations in face-centred cubic crystals ($\boldsymbol{b} = \frac{1}{3}\langle 111\rangle$) has been computed by Silcock and Tunstall (1964), following the earlier computations of Howie and Whelan (1962) of the contrast from partial dislocations. They found, in agreement with Howie and Whelan, that for $\boldsymbol{g}.\boldsymbol{b} = \pm\frac{1}{3}$ (where $\boldsymbol{g}$ is the reciprocal lattice vector corresponding to the Bragg reflection and $\boldsymbol{b}$ the Burgers vector of the dislocation) a Frank dislocation is invisible. However, they extended the computations of Howie and Whelan for $\boldsymbol{g}.\boldsymbol{b} = \pm\frac{2}{3}$, and showed that a Frank dislocation which is visible for $\boldsymbol{g}.\boldsymbol{b} = +\frac{2}{3}$ is invisible for $\boldsymbol{g}.\boldsymbol{b} = -\frac{2}{3}$, at large values of w (with $w = \xi_g s_g$, where ξ_g is the extinction distance and s_g the distance in reciprocal space of the operating reciprocal lattice point from the sphere of reflection). Further, computed profiles for 220 reflections indicated a very characteristic contrast. These profiles showed that the image of a Frank dislocation is double and that the intensity of the contrast oscillates with depth in the foil, giving a "dotted" appearance, with the image more intense at one surface of the foil than the other. By making use of the absence of contrast for 111 reflections, characteristic contrast for 220 reflections, and "reversal" of contrast for 020 and $0\bar{2}0$ reflections, Silcock and Tunstall were able to distinguish between Frank and Shockley ($\boldsymbol{b} = \frac{1}{6}\langle 112\rangle$) partial dislocations.

* Division of Tribophysics, CSIRO, University of Melbourne, Parkville, Vic. 3052.

In materials of low stacking fault energy, it is expected that a Frank dislocation lying along the $[1\bar{1}0]$ direction, for example, will dissociate into a Shockley partial dislocation and a low energy stair-rod dislocation according to the reaction

$$\tfrac{1}{3}[111] \rightarrow \tfrac{1}{6}[112] + \tfrac{1}{6}[110].$$

If such a dissociation occurs, then along the line of the original Frank dislocation there will be a Shockley and a stair-rod dislocation separated by an additional strip of stacking fault. The contrast from this combination of two dislocations and two stacking faults would be expected to differ from the contrast of the undissociated dislocation. It is of importance to be able to distinguish between dissociated and undissociated Frank dislocations, since the dissociation reaction is involved in the formation of other defects such as stacking fault tetrahedra from triangular Frank loops, and since growth and/or annealing of Frank dislocation loops by climb will probably be influenced by the degree of dissociation.

In this paper, theoretical images for undissociated and dissociated Frank dislocations are computed and compared, and the influence of the degree of dissociation and of w on the diffraction contrast for 111, 220, and 020 reflections investigated. It is shown that in many details the diffraction contrast from a dissociated Frank dislocation differs from that of an undissociated dislocation.

II. Image Computation

The computation of dislocation images was carried out using the computation technique developed originally by Head (1967), for single dislocations in untilted foils, and extended by Humble (1968) to deal with two parallel dislocations and up to three faulted planes in a foil of arbitrary orientation (hereinafter referred to as the Head–Humble technique). Restrictions imposed by the method of computation should be noted. Firstly, the stair-rod and Shockley partial dislocations resulting from dissociation of the Frank dislocation are required to be parallel. Secondly, surface relaxation effects cannot be taken into account using the Head–Humble computation technique since the speed of the method is based on the fact that the strain field of a (straight, infinite) dislocation is constant along any line parallel to the dislocation line. However, this latter restriction has not proved severe in the matching of images of dislocations in β-brass (Head 1967; Humble 1968). It should further be noted that the computer programme developed by Head uses the full anisotropic strain field of the dislocations in the contrast calculations.

A consistent method of denoting the Burgers vectors of dislocations and the shears resultant on a particular plane was required to ensure computation of physically realizable situations. Consider a section through a foil of arbitrary normal $\boldsymbol{FN}$ containing two parallel dislocations bounding three faulted planes, the section plane containing the beam direction $\boldsymbol{B}$ and the line $\boldsymbol{B} \times \boldsymbol{u}$, where $\boldsymbol{u}$ is a vector along the dislocation line. This section is the same used to develop the "generalized cross section" in the Head and Humble analyses. Two possible such sections are shown in Figure 1. Although planes 1, 2, and 3 in Figure 1(a) are parallel to the corresponding planes in Figure 1(b), it can be seen that two entirely different situations may arise.

The fault planes in Figure 1(*a*) include acute angles, whereas in Figure 1(*b*) they include obtuse angles. In the computation programme these differing geometrical arrangements are specified by denoting the normal to plane 2 as downward for the case shown in Figure 1(*a*) and upward for Figure 1(*b*). The positive sense of the dislocations is out of the paper and planes 1 and 3 are in the left- and right-most fields of the cross section respectively and are bounded by dislocations 1 (D1) and 2 (D2) respectively. Plane 2 joins dislocations 1 and 2. A dissociated Frank dislocation can be simulated by defining the shear on plane 1 (say) to be zero, planes 2 and 3 to be faulted {111} planes, dislocation 1 to be a Shockley partial, and dislocation 2 to be a stair-rod dislocation.

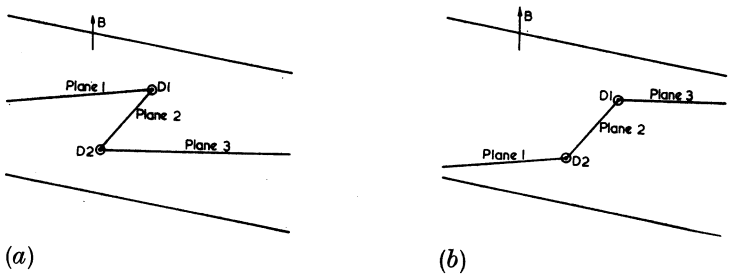

Fig. 1.—Geometrical arrangements of fault planes and dislocations used in image computation: (*a*) fault planes include acute angles, (*b*) fault planes include obtuse angles. D1 and D2 denote dislocations 1 and 2 respectively.

The rules given by Frank and Nicholas (1953) and Thompson (1953) concerning the development of intrinsic and extrinsic faulting and the shear resultant on a plane from the motion of a dislocation, together with the FS/RH rule (Frank 1951) for denoting the Burgers vector of a dislocation, provide the basis from which Burgers vectors of partial dislocations and the shears required to produce either intrinsic or extrinsic faulting can be deduced once the sense of the dislocation line has been established. In this investigation, the anticlockwise circuit about a dislocation loop is taken to be the positive direction of the dislocation. Thus the Burgers vector of the Frank dislocation and the shear, $\boldsymbol{R}$, resultant on the plane of the loop for an intrinsic (vacancy condensation) loop is upward drawn from the loop.* It should be noted further that, for the maintenance of continuity of the crystal, there is a fixed relationship between the Burgers vector of a dislocation and the shears resultant on faulted planes bounded by that dislocation.

In the theoretical computations, 7% below and 15% above background intensity have been taken as the visibility limits. That is, respectively darker and lighter characters than those used for background intensity in the halftone image come into operation at these visibility limits.

In most computations, use has been made of the facility in the extended computer programme (Humble 1968) to calculate the contrast from a selected portion only of a dislocation running from top to bottom of the foil. This has proved necessary to provide adequate resolution of image detail. Thus in various images the line spacing

* Following Art, Gevers, and Amelinckx (1963), the $\frac{1}{3}\langle 111\rangle$ "shear" notation has been used in all cases to denote the nature of the stacking fault being considered.

may correspond to different distances and for all images this "line resolution" is specified in the figure legends. The "character resolution" along any line is always six-tenths of the line resolution.

For image computation, the elastic stiffness constants for a copper–aluminium (9·98%) alloy (c_{11}, 15·95; c_{12}, 11·76; c_{44}, $7\cdot66\times10^{11}$ dynes cm^{-2}; Hearmon 1956) were used as being typical of a material of low stacking fault energy. The separation S of the stair-rod dislocation and the Shockley dislocation was expressed for computation as a fraction of the extinction distance for the operating reflection. In converting these separations to Angstrom units, the extinction distances given by Hirsch *et al.* (1965) for copper were used. In all computations a value of 0·1 has been used for anomalous and real absorption.

III. Theoretical Images

For the computation of all images, an intrinsically faulted Frank dislocation loop is taken on (111) with $\boldsymbol{b} = \frac{1}{3}[111]$ and the edge along $[10\bar{1}]$ considered. The dissociated combination consists of an intrinsic stacking fault on (111) bounded by the stair-rod dislocation with $\boldsymbol{b} = \frac{1}{6}[101]$ along $[10\bar{1}]$, and an intrinsic stacking fault on $(1\bar{1}1)$ bounded by the Shockley dislocation with $\boldsymbol{b} = \frac{1}{6}[121]$. For 111 and 020 reflections, a foil thickness t equivalent to $6\xi_{111}$ is used and the images are computed for the edge of the loop between $1\cdot5$ and $4\cdot5\xi_{111}$ from the top surface. For the 220 reflections the foil thickness is $6\xi_{220}$ and the edge of the loop is taken from the top to the bottom of the foil.

In discussing the different intensities present in the images, the word "contrast" will be used to denote intensities less than background and the terms "light" and "dark" to denote relative intensities within an image. Thus a fringe or other detail of an image may be described as "light" in the sense that it is a lighter shade than the neighbouring parts of the image without implying that the detail is brighter than background intensity. The term "reversal" will be used to indicate a change from "dark" to "light" or "light" to "dark" on changing the sense of the reflecting vector.

The theoretical images for 111, 220, and 020 reflections will be considered in turn. Further, since the combination of stacking faults resulting from dissociation may be overlapping or non-overlapping when viewed in the beam direction, the influence of beam direction on the contrast will be examined.

(*a*) *111 Reflections*

In considering 111 reflections, we will distinguish between the cases where the reflecting vector is normal to the dislocation line ($\boldsymbol{g}.\boldsymbol{u} = 0$) or inclined to it ($\boldsymbol{g}.\boldsymbol{u} \neq 0$).

(i) $\boldsymbol{g}.\boldsymbol{u} = 0$

For the case $\boldsymbol{g}.\boldsymbol{u} = 0$, the fault formed by dissociation is on a vertical plane containing the beam direction and rotations around the reflecting vector do not alter the configuration of the original fault and that due to dissociation. The images for the [110] beam direction and the $\bar{1}1\bar{1}$ and $1\bar{1}1$ reflections at $w = 0\cdot3$ (Fig. 2) indicate that no contrast occurs along $[10\bar{1}]$ either for the undissociated Frank or for any

value of S, the separation of the stair-rod and Shockley dislocations. However, there are several interesting effects associated with increasing S. As S starts to increase, the dark fringes tend to become pointed and develop "feathery" ends

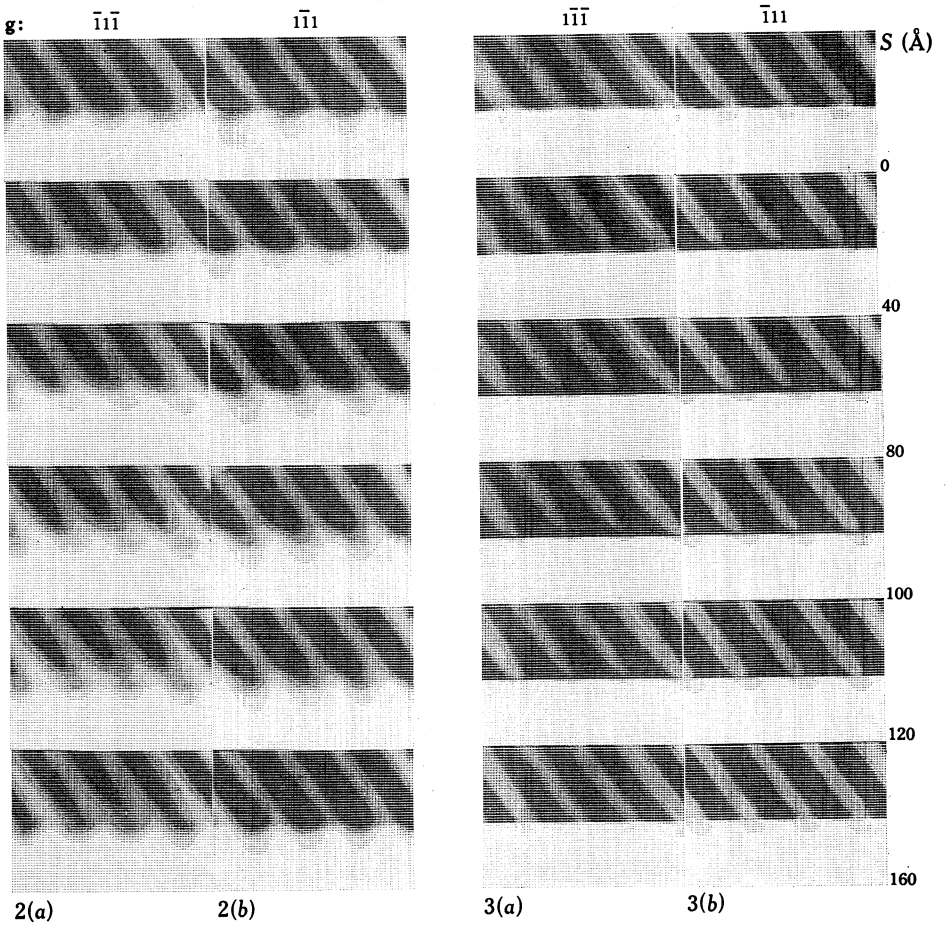

Figs 2 and 3.—Influence of the degree of dissociation and sense of the diffracting vector on the diffraction contrast from a Frank dislocation:

$$\boldsymbol{B}\,[110], \quad \boldsymbol{FN}\,[110], \quad w = 0{\cdot}3.$$

The values of S and $\boldsymbol{g}$ are indicated. Line resolution is 18 Å.

at the edge of the loop, whilst the intensity in the light fringes approaches background. These effects can be seen to reverse as S increases further. There is no pronounced influence of w on these phenomena in the range of w from 0 to 0·9 and the phenomena are essentially the same for $+\boldsymbol{g}$ and $-\boldsymbol{g}$. It is of interest that these contrast effects arise with $\boldsymbol{g}.\boldsymbol{b} = 0$ for the Shockley, $\pm\frac{1}{3}$ for the stair-rod, and with $\boldsymbol{g}.\boldsymbol{R} = \pm 1$ for the fault on the vertical plane, i.e. with both dislocations and the fault formed by dissociation nominally out of contrast.

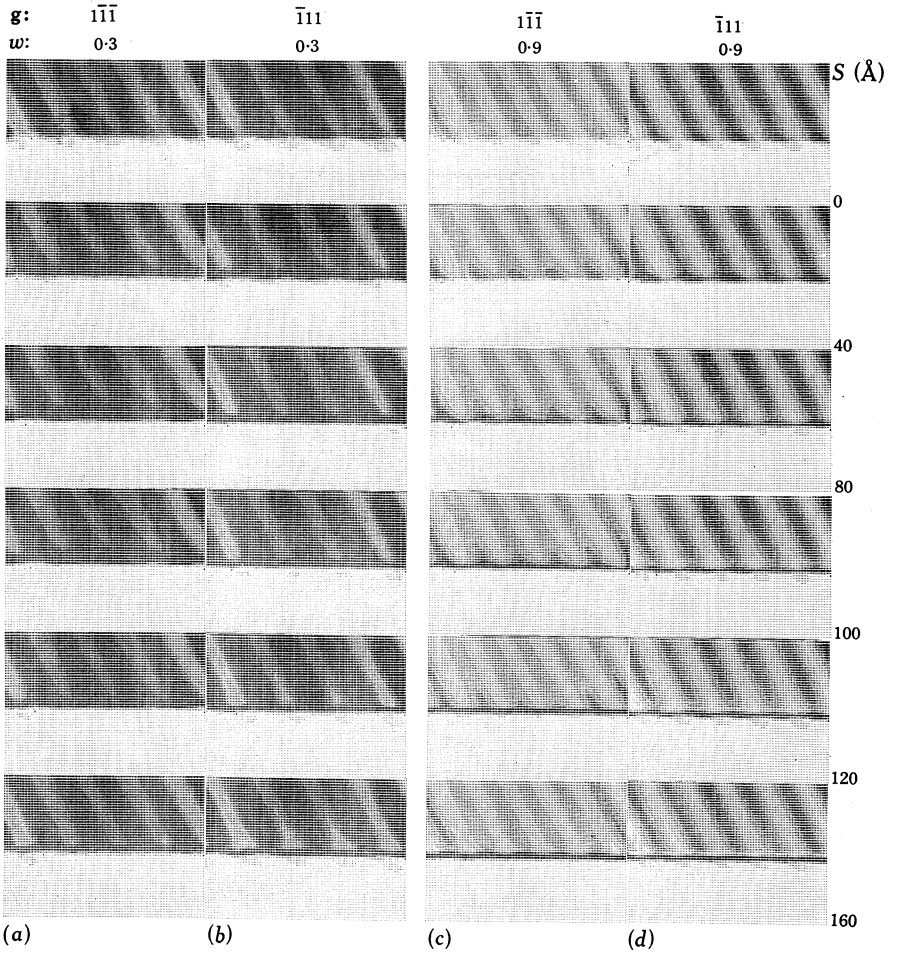

Fig. 4.—Influence of the degree of dissociation, sense of the diffracting vector, and w on the diffraction contrast from a Frank dislocation:

$$\boldsymbol{B}\,[211], \qquad \boldsymbol{FN}\,[110].$$

The values of S, $\boldsymbol{g}$, and w are indicated. Line resolution is 19 Å.

(ii) $\boldsymbol{g}.\boldsymbol{u} \neq 0$

For the case $\boldsymbol{g}.\boldsymbol{u} \neq 0$, the fault formed by dissociation can be on a vertical plane containing the beam direction, but rotations around the reflecting vector move the beam direction so as to result in overlapping or non-overlapping faults, and each of these cases will be considered in turn. For the theoretical images in Figures 3 and 4, the fault on $(1\bar{1}1)$ due to the separation of the Shockley and stair-rod has $\boldsymbol{g}.\boldsymbol{R} = \pm\frac{1}{3}$. For the Shockley $\boldsymbol{g}.\boldsymbol{b} = \pm\frac{1}{3}$ and for the stair-rod $\boldsymbol{g}.\boldsymbol{b} = 0$.

Figure 3(a) shows the images for the $[110]$ beam direction and the $1\bar{1}\bar{1}$ reflection. For the undissociated case, no contrast is observed at the Frank dislocation along $[10\bar{1}]$. However, as S increases, contrast is observed along this edge of the loop. This contrast appears to develop by the dark fringes widening at the edge of the

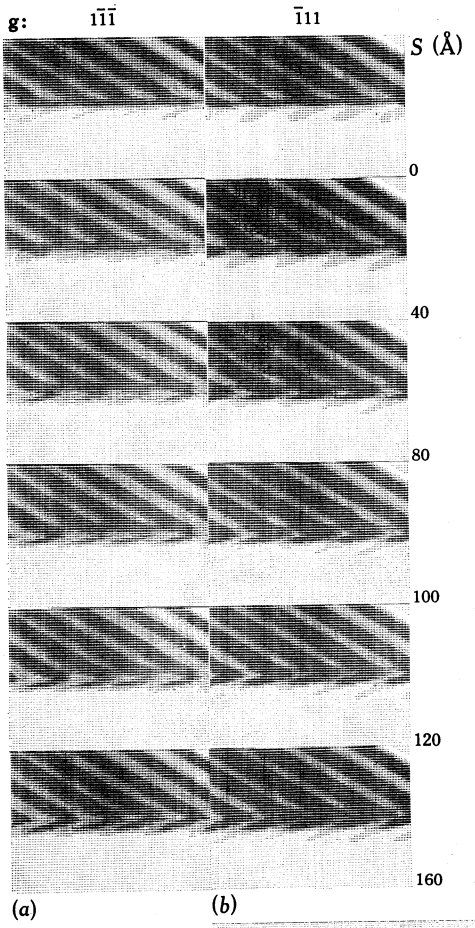

Fig. 5.—Influence of the degree of dissociation and sense of the diffracting vector on the diffraction contrast from a Frank dislocation:

$\boldsymbol{B}$ $[12\bar{1}]$,
$\boldsymbol{FN}$ $[110]$,
$w = 0\cdot3$.

The values of S and $\boldsymbol{g}$ are indicated. Line resolution is 16 Å.

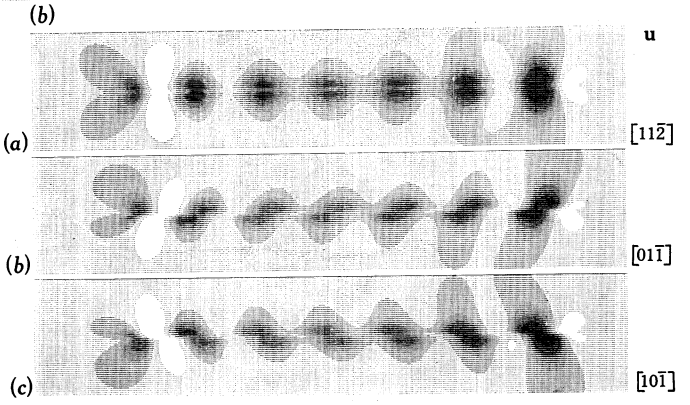

Fig. 6.—Influence of $\boldsymbol{u}$ on the 220 contrast from an undissociated Frank dislocation:

$\boldsymbol{B}$ $[110]$, $\boldsymbol{FN}$ $[110]$, $\boldsymbol{g}$ $[\bar{2}20]$, $w = 0\cdot3$.

Line resolution is 15 Å in (*a*) and 18 Å in (*b*) and (*c*).

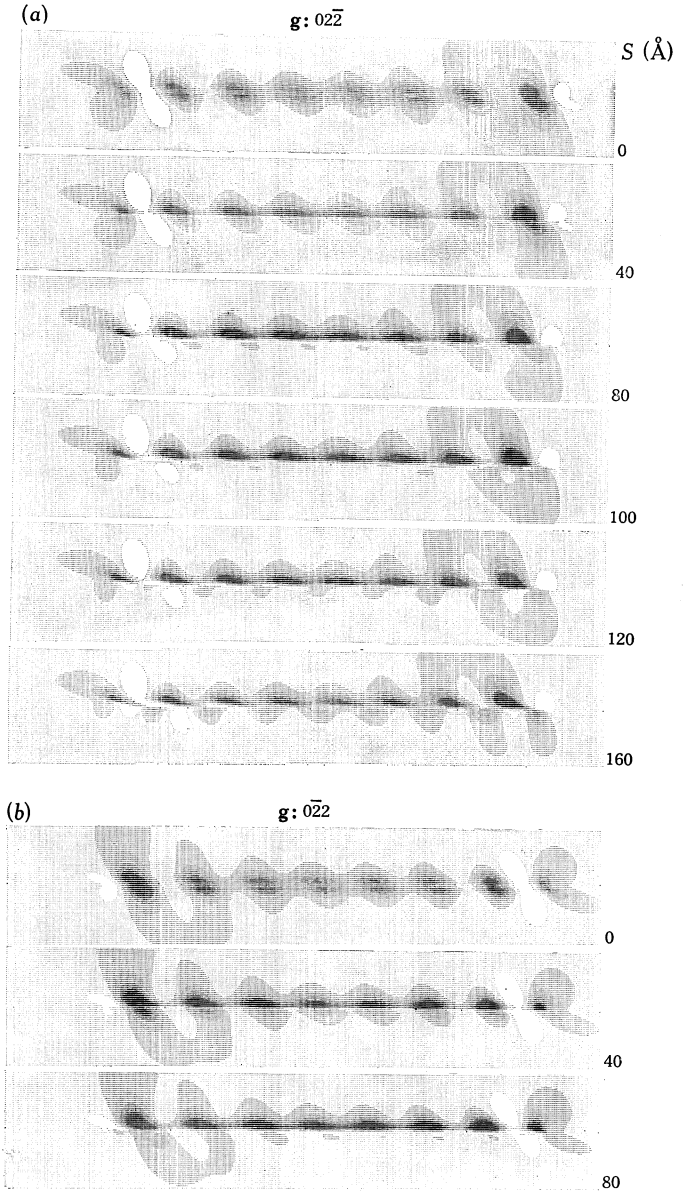

Fig. 7.—Influence of the degree of dissociation and sense of the diffracting vector on the diffraction contrast from a Frank dislocation:

$$\boldsymbol{B}\,[211], \quad \boldsymbol{FN}\,[110], \quad w = 0{\cdot}3.$$

The values of S and $\boldsymbol{g}$ are indicated. Line resolution is 18 Å.

loop and, for the cases shown, the effect is most pronounced at $w = 0 \cdot 3$ and $S = 80$ Å. As S increases beyond 80 Å, the dark fringes start to narrow again. This effect is less pronounced near the surfaces of the foil and at large values of w. Similar changes in the images occur for the $\bar{1}11$ reflection; however, in this case the contrast along the edge of the loop is clearer, as the fringes do not broaden to such an extent (Fig. 3(*b*)).

The images in Figure 4 are for the [211] beam direction, a case where the fault formed by the dissociation of the Frank dislocation is on a plane inclined to the beam direction, so that the fault due to the dissociation and the fault in the original loop overlap. As can be seen, there is only very weak contrast for the undissociated Frank dislocation in either $+\boldsymbol{g}$ or $-\boldsymbol{g}$. However, for $S = 40$ Å, contrast is present at the edge of the loop and is maintained at all values of S and w. The topology of the fault fringes at the edge of the dissociated loop varies with S and the sense of the reflecting vector.

The images in Figure 5 are for the $[12\bar{1}]$ beam direction, a case where the fault formed by dissociation is on a plane inclined to the beam direction, so that the fault formed by dissociation and that in the original loop do not overlap. Here, even the undissociated Frank gives contrast. The main effect of dissociation in this case is the development of a set of fringes on $(1\bar{1}1)$ which can be detected at $S = 40$ Å and are clear at $S = 80$ Å. The fringes on $(1\bar{1}1)$ are more pronounced at all separations for the $\bar{1}11$ reflection than for the $1\bar{1}\bar{1}$ reflection.

In general, the computations of 111 contrast for the undissociated Frank dislocation for the orientations considered in Figures 2–4 confirm previous conclusions that no contrast is observed for $\boldsymbol{g}.\boldsymbol{b} = \pm\frac{1}{3}$ (Howie and Whelan 1962; Silcock and Tunstall 1964). However, the results in Figure 5 show that contrast does occur for $\boldsymbol{g}.\boldsymbol{b} = \pm\frac{1}{3}$ and indicate that 111 contrast for an undissociated Frank is sensitive to the beam direction.

(*b*) *220 Reflections*

The profiles computed by Silcock and Tunstall (1964) indicate that an undissociated Frank dislocation has a very characteristic image for 220 reflections for which $\boldsymbol{g}.\boldsymbol{R}$ is an integer. The topology suggested by the profiles is a series of double dots running through the foil with the intensity approaching background along the line of the dislocation. Further, the intensity is greater at one surface than at the other. The case considered by Silcock and Tunstall, for a $\boldsymbol{u}$ along $\langle 112 \rangle$, is presented as a computed image in Figure 6(*a*). It is clear that the topology suggested by their profiles is confirmed. The image for this particular geometry is little affected by varying w, except for values of w, at which an additional double dot is developing in the image, when a portion of the image appears to be double and continuous.

For Frank dislocation loops in quenched specimens, the edges of the loops lie along $\langle 110 \rangle$ rather than $\langle 112 \rangle$ directions, so that we will only consider here images of dislocations lying along $\langle 110 \rangle$. Computed images for undissociated Frank dislocations with $\boldsymbol{u}$ along $[01\bar{1}]$ and along $[10\bar{1}]$ are shown in Figures 6(*b*) and 6(*c*) respectively. It can be seen that the major effect of altering $\boldsymbol{u}$ from $\langle 112 \rangle$ to $\langle 110 \rangle$ is to "shear" the main features of the contrast so that they are inclined to the line of the dislocation. Images of dislocations along $[01\bar{1}]$ and $[10\bar{1}]$ are related by reflection about the line of the dislocation.

Theoretical images of a dissociated Frank dislocation along $[10\bar{1}]$ for the reflections $02\bar{2}$ and $0\bar{2}2$ are given in Figure 7. For these images the fault arising from the dissociation is inclined to the beam direction with $\boldsymbol{g}.\boldsymbol{R} = \pm\frac{4}{3}$ and the Shockley and stair-rod dislocations have $\boldsymbol{g}.\boldsymbol{b} = \pm\frac{1}{3}$. The immediate influence of dissociating the Frank dislocation is to enhance the image at one side of the dislocation at the expense of the other, and at $S = 80$ Å, for example, the image is almost completely on one side, apart from the regions of low contrast near the surfaces of the foil (Fig. 7(*a*)). Further, the image, although dotted, is much more continuous than that for the undissociated Frank. With increasing S, contrast appears again on both sides of the dislocation.

The general character of the images for dissociated Frank dislocations for 220 reflections does not alter greatly with change in w. The main effects of increasing w, in the range from 0 to $0\cdot9$, are that the intensity of the image decreases and it tends to become continuous at smaller separations.

The images for undissociated Frank dislocations invert from top to bottom of the foil and from side to side of the dislocation on changing the operative reflection from $+\boldsymbol{g}$ to $-\boldsymbol{g}$. Contrary to this behaviour, the image of a dissociated Frank dislocation does not invert in this way (compare Figs 7(*a*) and 7(*b*)). The image retains its asymmetry with the contrast on the same side of the dislocation in both $+\boldsymbol{g}$ and $-\boldsymbol{g}$ except for regions of low contrast near the surfaces of the foil. However, there is an inversion of the major features (but not the fine detail) of the contrast from top to bottom of the foil.

Images similar to those given in Figure 7, but less continuous for similar values of S, are obtained for the $2\bar{2}0$ reflection in the $[110]$ beam direction for which the fault on $(1\bar{1}1)$, with $\boldsymbol{g}.\boldsymbol{R} = \pm\frac{4}{3}$, is on a vertical plane.

Computed images of undissociated and dissociated Frank dislocations for 220 reflections and the same foil thickness used for 111 and 020 reflections show the same characteristics as those given here.

(*c*) *002 Reflections*

The computations of Silcock and Tunstall (1964) indicate that, for an undissociated Frank dislocation, the contrast for 002 reflections is comparatively simple; the dislocation being in contrast for $\boldsymbol{g}.\boldsymbol{b} = +\frac{2}{3}$ and out of contrast for $\boldsymbol{g}.\boldsymbol{b} = -\frac{2}{3}$, at large values of w. Computed images for undissociated Frank dislocations are shown in the top rows of Figures 8–13. In all cases, contrast is present for $\boldsymbol{g}.\boldsymbol{b} = \pm\frac{2}{3}$ at $w = 0\cdot3$ but, for values of w of $0\cdot6$ and $0\cdot9$ and $\boldsymbol{g}.\boldsymbol{b} = -\frac{2}{3}$, no contrast is observed at the dislocation where it crosses a light fringe. These computed images are thus in agreement with the profiles computed by Silcock and Tunstall. However, this simple reversal of contrast does not apply where the dislocation crosses a dark fringe.

In considering the dissociated dislocation, as for 111 reflections, we will distinguish between two cases for 002 reflections, namely $\boldsymbol{g}.\boldsymbol{u} = 0$ and $\boldsymbol{g}.\boldsymbol{u} \neq 0$.

(i) $\boldsymbol{g}.\boldsymbol{u} = 0$

For $\boldsymbol{g}.\boldsymbol{u} = 0$, the original fault and that formed by dissociation always overlap to the same extent for the usual experimental rotations around the direction of the reflecting vector. The $[100]$ beam direction is used in these computations and, for

$\boldsymbol{u}$ along $[10\bar{1}]$, $\boldsymbol{g}.\boldsymbol{u} = 0$ for the 020 and $0\bar{2}0$ reflections. Here, $\boldsymbol{g}.\boldsymbol{R} = \pm\frac{2}{3}$ for the original fault and for the fault formed by dissociation, $\boldsymbol{g}.\boldsymbol{b} = \pm\frac{2}{3}$ for the Shockley dislocation, and $\boldsymbol{g}.\boldsymbol{b} = 0$ for the stair-rod dislocation.

Theoretical images for the 020 and $0\bar{2}0$ reflections for various values of S and w are given in Figure 8. The most noticeable effect of dissociation on the image for the 020 reflection is that a light band between the stacking fault fringes and the edge of the loop, which is not clearly defined for the undissociated Frank, becomes pronounced. With increasing S this light band remains a prominent feature of the 020 image. Such a light band is not a feature of the $0\bar{2}0$ images. However, as S increases beyond 40 Å strong contrast appears at the edge of the loop for the $0\bar{2}0$ reflection, at all values of w, so that there is no reversal of contrast on $+\boldsymbol{g}$ and $-\boldsymbol{g}$.

For the 020 reflection and values of S greater than 100 Å contrast appears between the dark fringes on the inner or Shockley side of the light band and this contrast varies with S and w. At large separations the 020 image at the edge of the loop could be described as two dark lines separated by a light band, whereas the $0\bar{2}0$ image appears as a single dark line. Thus for a dissociated Frank dislocation with $\boldsymbol{g}.\boldsymbol{u} = 0$, the contrast for 002 reflections does not reverse on $+\boldsymbol{g}$ and $-\boldsymbol{g}$ in the simple manner found for an undissociated Frank. Rather, the contrast of the dissociated Frank is a sensitive function of the sense of $\boldsymbol{g}$, the separation of the partials, and of w.

(ii) $\boldsymbol{g}.\boldsymbol{u} \neq 0$

In contrast to the case for $\boldsymbol{g}.\boldsymbol{u} = 0$, when $\boldsymbol{g}.\boldsymbol{u} \neq 0$ the configuration of the faults changes rapidly for rotations around the reflecting vector and gives rise to marked changes in the image for dissociated Frank dislocations. For the geometry chosen, a rotation around the reflecting vector so as to alter the beam direction from [100] to [110] reduces the overlap of the original fault and that resulting from dissociation from a maximum value to zero, whilst continued rotation in the same sense from [110] to [010] exposes both faults individually when viewing in the electron beam direction. Theoretical images for this whole range of rotation will be discussed here. The operative reflections in all beam directions are 002 and $00\bar{2}$, which give $\boldsymbol{g}.\boldsymbol{R} = \pm\frac{2}{3}$ for the original fault and that formed by dissociation, $\boldsymbol{g}.\boldsymbol{b} = \pm\frac{1}{3}$ for the Shockley partial, and $\boldsymbol{g}.\boldsymbol{b} = \pm\frac{1}{3}$ for the stair-rod partial.

Figure 9 shows theoretical images for the [100] beam direction for various values of S and w. Although these images are similar in some respects to the 020 images in Figure 8, they differ in detail. A light band between the stacking fault fringes and the edge of the loop is present for the 002 reflection but only at values of S greater than 100 Å. As for the 020 reflection, an inner dark line develops for the 002 reflection at large values of S, but it is always weaker than for the 020 reflection.

Strong contrast along the edge of the loop for the $00\bar{2}$ reflection does not occur until values of S of approximately 100 Å and the exact value of S at which this contrast appears is a function of w. Thus for $\boldsymbol{g}.\boldsymbol{u} \neq 0$, reversal of contrast persists to larger separations of the Shockley and stair-rod dislocations than for $\boldsymbol{g}.\boldsymbol{u} = 0$.

Figures 10 and 11 show how the contrast along the edge of the loop, for various values of S, alters as the beam direction is changed from [100] through [310], [210], [650], to [110]. Comparisons of the images for these different beam directions are made for the value of w of $0\cdot6$ only. In all cases in Figures 10 and 11 the foil normal

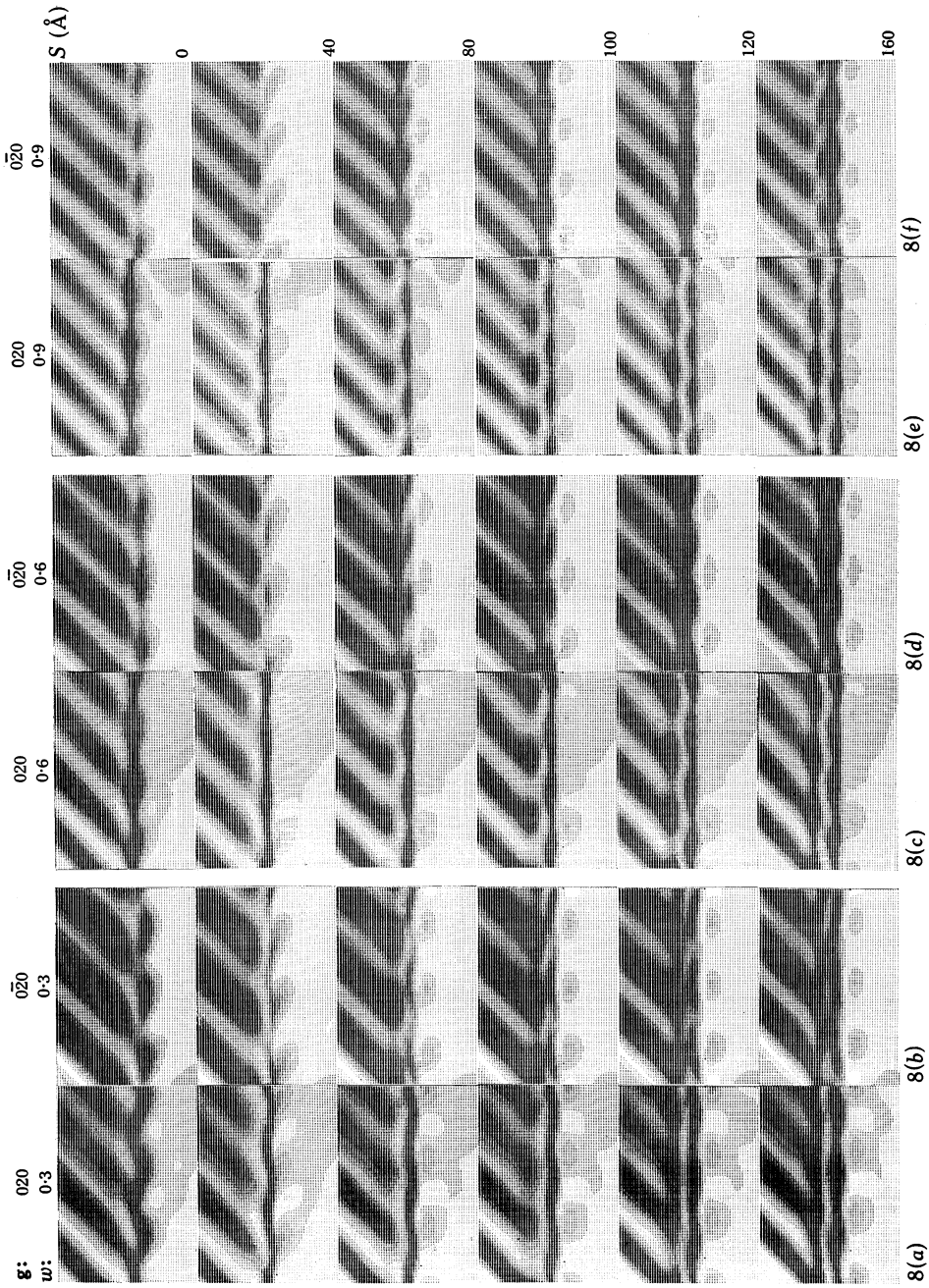
g:
m:
020
0·3
$0\bar{2}0$
0·3
020
0·6
$0\bar{2}0$
0·6
020
0·9
$0\bar{2}0$
0·9
S (Å)
0
40
80
100
120
160
8(a)
8(b)
8(c)
8(d)
8(e)
8(f)

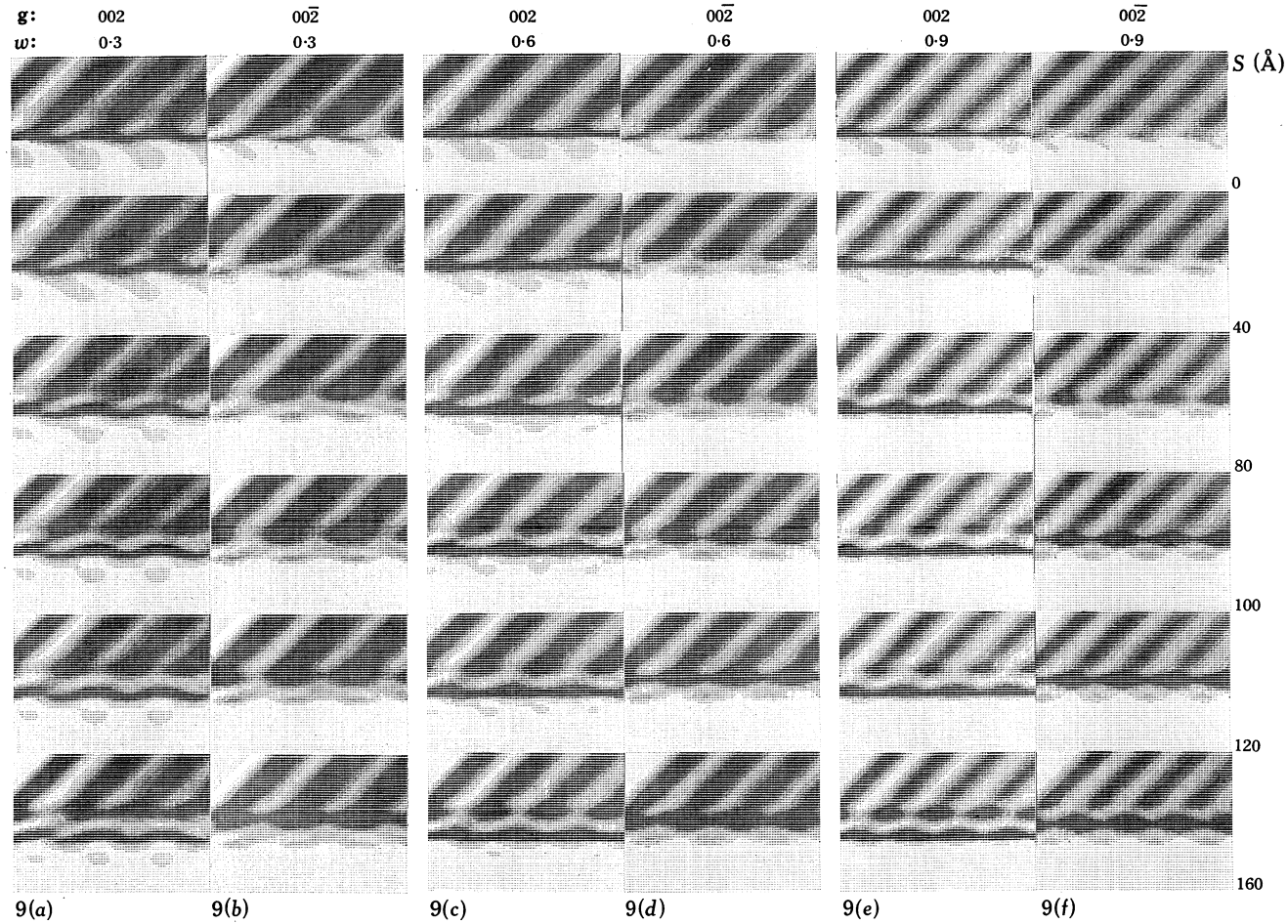

Figs 8 and 9.—Influence of the degree of dissociation, sense of the diffracting vector, and w on the diffraction contrast from a Frank dislocation:

B [100], ***FN*** [100].

The values of S, $\boldsymbol{g}$, and w are indicated. Line resolution is 10 Å.

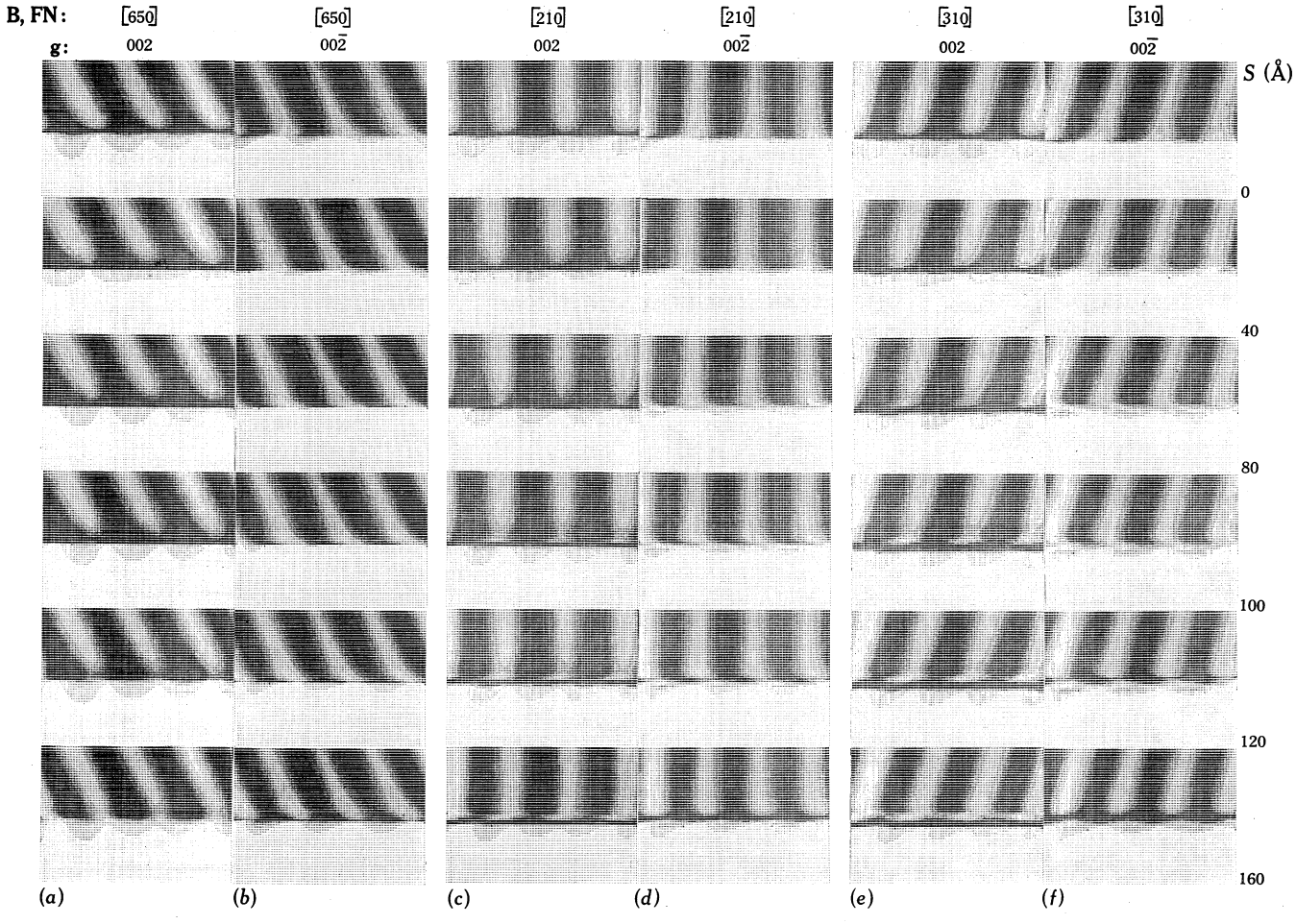

Fig. 10.—Influence of the beam direction, degree of dissociation, and sense of the diffracting vector on the diffraction contrast from a Frank dislocation:

$w = 0 \cdot 6$, ***B*** and ***FN*** coincident.

The values of S, ***B*** (***FN***), and ***g*** are indicated. Line resolution is 16 Å in (*a*) and (*b*), 12 Å in (*c*) and (*d*). and 11 Å in (*e*) and (*f*).

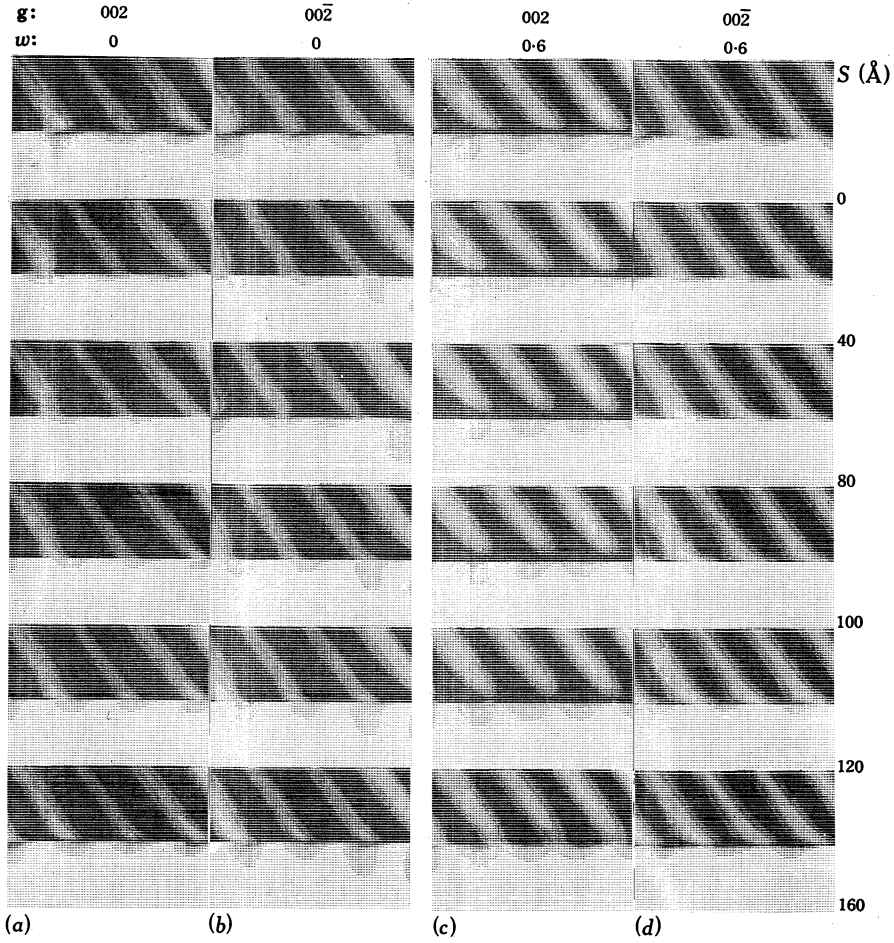

Fig. 11.—Influence of the degree of dissociation, sense of the diffracting vector, and w on the diffraction contrast from a Frank dislocation:

B [110], ***FN*** [110].

The values of S, $\boldsymbol{g}$, and w are indicated. Line resolution is 18 Å.

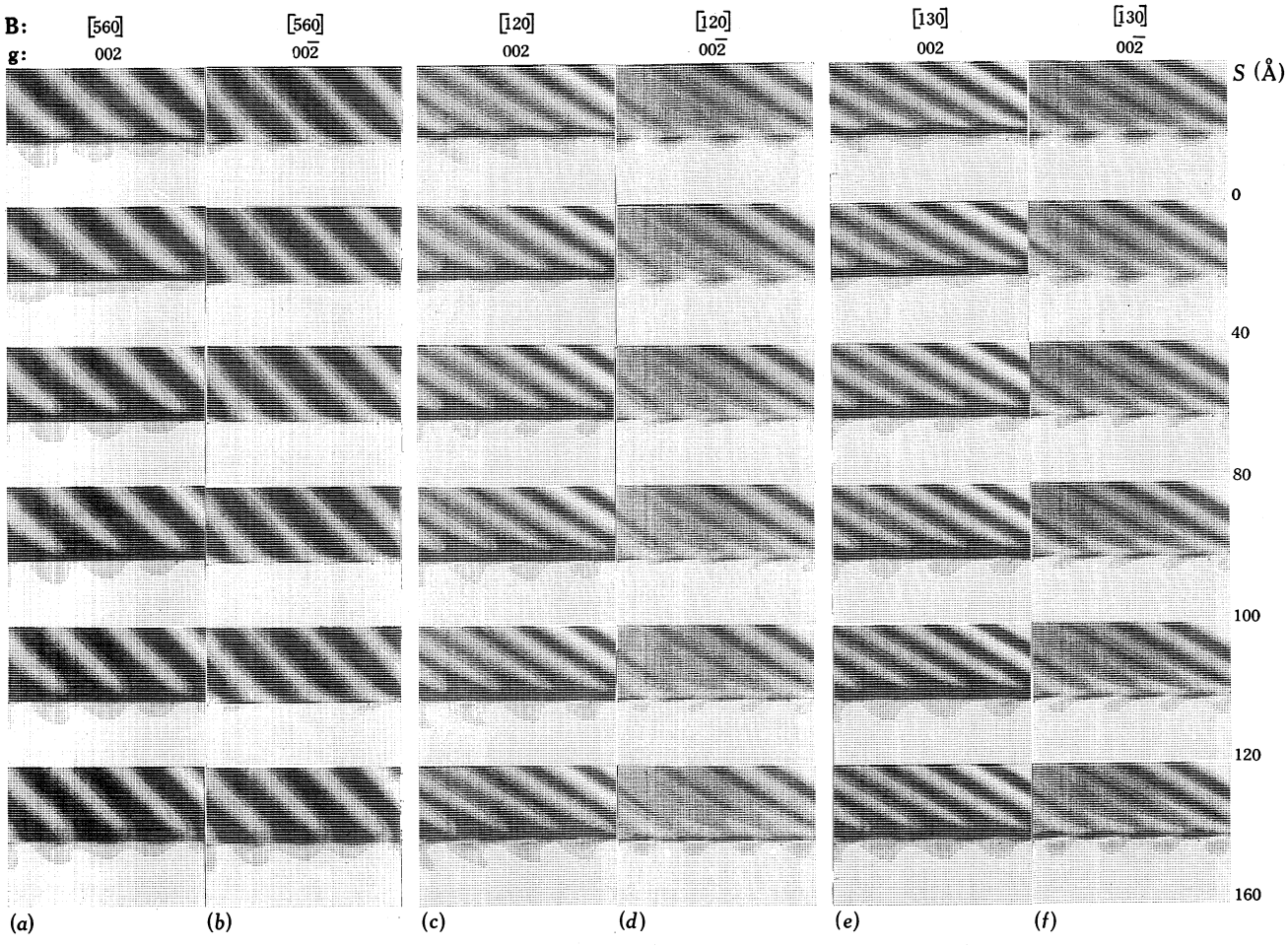

Fig. 12.—Influence of the beam direction, degree of dissociation, and sense of the diffracting vector on the diffraction contrast from a Frank dislocation:

$$w = 0 \cdot 6, \quad \boldsymbol{FN}\ [560]\ ((a) \text{ and } (b)), \quad \boldsymbol{FN}\ [12\bar{1}]\ ((c)\text{–}(f)).$$

The values of S, $\boldsymbol{B}$, and $\boldsymbol{g}$ are indicated. Line resolution is 21 Å in (a) and (b) and 17 Å in (c)–(f).

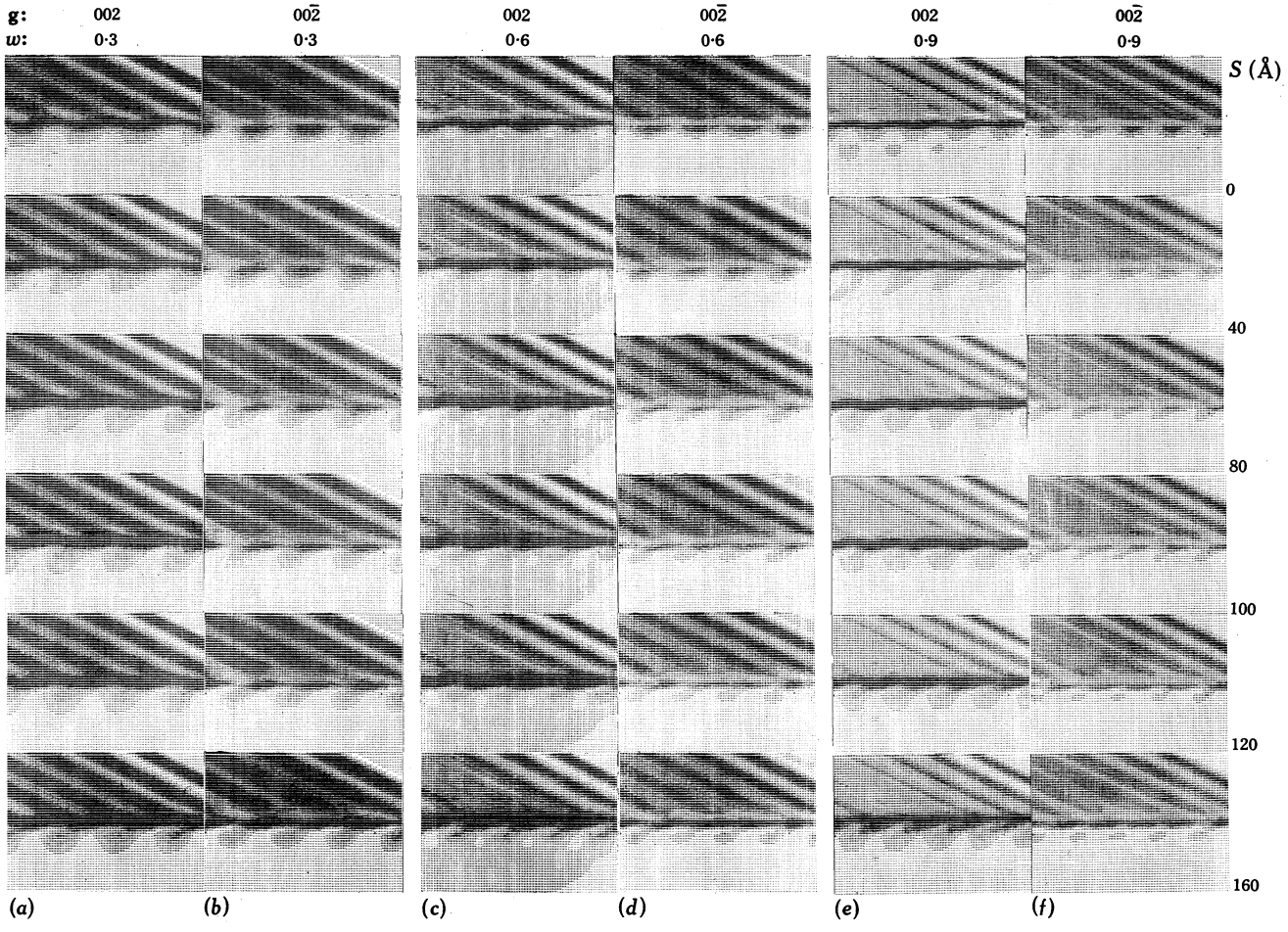

Fig. 13.—Influence of the degree of dissociation, sense of the diffracting vector, and w on the diffraction contrast from a Frank dislocation:

$\boldsymbol{B}$ [010], $\boldsymbol{FN}$ [12$\bar{1}$].

The values of S, $\boldsymbol{g}$, and w are indicated. Line resolution is 17 Å.

is the same as the beam direction. Computations have shown that, apart from changes in fringe direction, there is little influence of foil normal on the detail of the image, provided that the line resolution is maintained.

Several changes in the images result from the change in beam direction from [100] to [110]. The main effect is that reversal of contrast continues to larger values of S as the beam direction approaches [110]; e.g. for [210] reversal of contrast persists to a value of S of 100 Å, whereas in [100] the corresponding value of S is 80 Å.

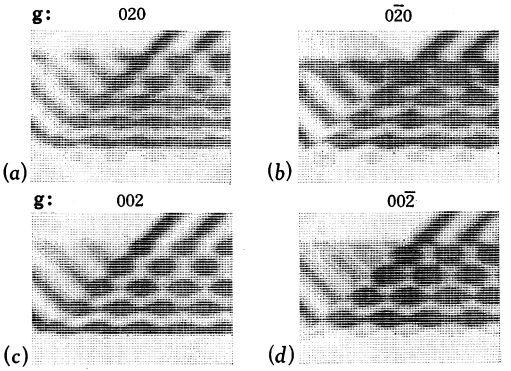

Fig. 14.—Diffraction contrast from a dissociated Frank dislocation for a separation S of the stair-rod and Shockley dislocations of 562 Å.

$\boldsymbol{B}$ [100],
$\boldsymbol{FN}$ [100],
$w = 0 \cdot 9$.

The values of $\boldsymbol{g}$ are indicated. Line resolution is 12 Å.

An anomolous effect occurs for the [650] beam direction in that at the largest value of S the contrast at the edge of the loop disappears for the 002 reflection and a fine line of contrast appears for the 00$\bar{2}$ reflection. The same phenomenon occurs in the [110] beam direction. This behaviour is opposite to that of an undissociated Frank dislocation and of a dissociated Frank dislocation in other beam directions.

For the [110] beam direction, the images at values of w of $0 \cdot 3$ and $0 \cdot 9$ are very similar to those at $w = 0 \cdot 6$. However, for the [110] beam direction at $w = 0$ (Figs 11(a) and 11(b)), the images are unusual in that very little contrast occurs at the edge of the loop for 002 or 00$\bar{2}$ for the undissociated Frank and no contrast for the dissociated Frank at all separations, except $S = 160$ Å, where a very fine dark line (approximately 20 Å) occurs along the edge of the loop for 002 and 00$\bar{2}$.

Thus rotation of the beam direction from [100] to [110] may result in a complete change in the contrast behaviour of a dissociated Frank dislocation for which $\boldsymbol{g}.\boldsymbol{u} \neq 0$, in that for large separations the dissociated dislocation exhibits reversal of contrast for $\pm\boldsymbol{g}$ in [110], whereas for [100] the dissociated dislocation does not exhibit reversal of contrast for $\pm\boldsymbol{g}$.

Figures 12 and 13 show how the contrast along the edge of the loop, for various separations of the partials, alters as the beam direction changes from [110] through [560], [120], [130], to [010]. The foil normal and beam direction are coincident for [560], but for the other beam directions a [12$\bar{1}$] foil normal has been used as this maintains an approximately constant line resolution similar to that in Figures 9–11. Dissociation results in non-overlapping faults for these beam directions. Comparisons of the images are made for $w = 0 \cdot 6$.

For the [560] beam direction, the images are very similar in 002 and 00$\bar{2}$ to those for the [650] beam direction, but for 002 the contrast along the edge of the loop remains strong until larger separations in the [560] beam direction than in the [650]

beam direction. For the [120] beam direction, the contrast along the edge of the loop for 002 is broader than for the [210] beam direction. For the [130] beam direction, the contrast along the edge of the loop is strong for all separations in 002. The reversal of contrast in $00\bar{2}$ is not as pronounced in [130] as in [310] because fine regions of contrast develop across the light fringes at the edge of the loop as S increases.

The images for the [010] beam direction at $w = 0 \cdot 6$ (Figs 13(*c*) and 13(*d*)) differ from the images in the [100] beam direction (Fig. 9) in several ways. In the [010] beam direction, the undissociated Frank dislocation shows a light band between the contrast at the edge of the loop and the fault fringes in both 002 and $00\bar{2}$. In contrast to the images for the [100] beam direction, the light band disappears at $S = 40$ Å and does not appear again at any of the separations computed for 002, whereas it remains a feature of the image for $00\bar{2}$. At $w = 0 \cdot 6$ image reversal is less pronounced at small values of S in 002 and $00\bar{2}$ for the [010] beam direction than for the [100] beam direction. At $S = 160$ Å, the start of a system of fringes on $(1\bar{1}1)$ can be seen and computations at a separation of two extinction distances show fringes due to the fault on $(1\bar{1}1)$.

Figure 13 includes computed images for the [010] beam direction at values of w of $0 \cdot 3$ and $0 \cdot 9$. The light band contrast for the undissociated Frank is absent at $w = 0 \cdot 3$ and less clear at $w = 0 \cdot 9$ due to fading of the fringe contrast. The broadening of the 002 images along the edge of the loop with increasing S can be seen, from an examination of the images at the three values of w, to be associated with the development of a new set of fringes on $(1\bar{1}1)$, the resolution of these fringes increasing with increasing w. As for the undissociated Frank, the extent to which the image of the dissociated Frank reverses in 002 and $00\bar{2}$ is sensitive to w, the reversal being more pronounced at large than at small values of w.

The main feature of rotations that result in non-overlapping faults is that the contrast is stronger in the 002 images than for rotations producing overlapping faults. For the former rotations an additional set of fringes appears at large separations.

For both $\boldsymbol{g}.\boldsymbol{u} = 0$ and $\boldsymbol{g}.\boldsymbol{u} \neq 0$ and for beam directions corresponding to overlapping faults, a light band parallel to the stair-rod dislocation becomes a characteristic feature of the images at large separations. Computations at separations of one and two extinction distances (Fig. 14) and for the [100] beam direction, for which the faults overlap, indicate that this light band is related to the characteristic fringe pattern parallel to the line of intersection of the fault planes of overlapping faults (Gevers, Art, and Amelinckx 1964). As can be seen from Figure 14, the fringe pattern parallel to the line of intersection shows reversal of dark for light on changing from $+\boldsymbol{g}$ to $-\boldsymbol{g}$ for $\boldsymbol{g}.\boldsymbol{u} \neq 0$, but not for $\boldsymbol{g}.\boldsymbol{u} = 0$. Comparison of Figure 14 with Figures 8(*e*) and 8(*f*) and 9(*e*) and 9(*f*) shows that, at separations greater than about 100 Å, the contrast of a dissociated Frank dislocation becomes dominated by the contrast from overlapping stacking faults.

(*d*) *Summary of Contrast Features*

The most striking features of the contrast from dissociated Frank dislocations which distinguish them from undissociated dislocations are as follows.

(1) For 111 reflections, strong contrast occurs when $\boldsymbol{g}.\boldsymbol{u} \neq 0$.

(2) For 220 reflections, images are single and continuous with strong contrast on one side only. The strong contrast does not invert from side to side for $+\boldsymbol{g}$ and $-\boldsymbol{g}$.

(3) For 020 reflections the extent to which reversal of contrast occurs in $\pm\boldsymbol{g}$ is a function of $\boldsymbol{g}$, S, and the beam direction. The sense of $\boldsymbol{g}$ for which a white band appears between the edge of the loop and the fault fringes is reversed on changing from overlapping to non-overlapping faults.

IV. Discussion

It is clear from the images presented here that the contrast from a Frank dislocation alters markedly on dissociation. Changes in the image are readily detectable at a separation of the Shockley and stair-rod dislocations of 40 Å, so that dissociation should be observable by diffraction contrast from Frank dislocation loops in silver and alloys with lower stacking fault energies.

The displacement field around a dislocation of a particular Burgers vector and hence the diffraction contrast is determined by the ratios of the elastic constants, $A = 2c_{44}/(c_{11}-c_{12})$ and $B = (c_{11}+2c_{12})/c_{44}$. Although the images presented here have been computed using the elastic constants of a copper–aluminium alloy, the values of A and B for this material are similar to those for silver, copper, and nickel and thus the computations should be equally applicable to these pure metals. To check whether the images would apply more generally to materials with quite different elastic constants, the contrast from undissociated and dissociated Frank dislocations has been computed for aluminium and an iron–nickel (30%) alloy, thereby covering the range of anisotropy of the common face-centred cubic metals and alloys. The general features of the contrast for these materials are very similar to those presented here for the copper–aluminium alloy and the present results are therefore applicable to most face-centred cubic metals and alloys. Experimental examples of contrast from Frank dislocation loops are given in Part II (present issue, pp. 371–91).

V. Acknowledgments

We are indebted to Dr. P. Humble for the use of his computer programme, which he developed to treat problems of the type investigated here, and to him and Dr. A. K. Head for many helpful discussions. We are extremely grateful to Mr. E. G. Beckhouse for photographic work.

VI. References

Art, A., Gevers, R., and Amelinckx, S. (1963).—*Phys. Status Solidi* **3**, 697.
Frank, F. C. (1951).—*Phil. Mag.* **42**, 809.
Frank, F. C., and Nicholas, J. F. (1953).—*Phil. Mag.* **44**, 1213.
Gevers, R., Art, A., and Amelinckx, S. (1964).—*Phys. Status Solidi* **7**, 605.
Head, A. K. (1967).—*Aust. J. Phys.* **20**, 557.
Hearmon, R. F. S. (1956).—*Adv. Phys.* **5**, 323.
Hirsch, P. B., Howie, A., Nicholson, R. B., Pashley, D. W., and Whelan, M. J. (1965).—"Electron Microscopy of Thin Crystals." p. 496. (Butterworths: London.)
Howie, A., and Whelan, M. J. (1962).—*Proc. R. Soc.* A **267**, 206.
Humble, P. (1968).—*Aust. J. Phys.* **21**, 325.
Silcock, J. M., and Tunstall, W. J. (1964).—*Phil. Mag.* **10**, 361.
Thompson, N. (1953).—*Proc. phys. Soc.* B **66**, 481.